Tribol Lett (2014) 56:481–490
DOI 10.1007/s11249-014-0425-x

ORIGINAL PAPER

Effects of Interfacial Bonding on Friction and Wear at Silica/Silica Interfaces

Ao Li · Yun Liu · Izabela Szlufarska

Received: 7 July 2014 / Accepted: 23 September 2014 / Published online: 2 October 2014

Abstract Static friction between amorphous silica surfaces with a varying number of interfacial siloxane (Si–O–Si) bridges was studied using molecular dynamic simulations. Static friction was found to increase linearly with the applied normal pressure, which can be explained in the framework of Prandlt–Tomlinson's model. Friction force was found to increase with concentration of siloxane bridges, but with a decreasing gradient, with the latter being due to interactions between neighboring siloxane bridges. In addition, we identified atomic-level wear mechanisms of silica. These mechanisms include both transfer of individual atoms accompanied by breaking interfacial siloxane bridges and transfer of atomic cluster initialized by rupturing of surface Si–O bonds. Our simulations showed that small clusters are continually formed and dissolved at the sliding interface, which plays an important role in wear at silica/silica interface.

Keywords Silica wear · Frictional aging · Molecular dynamics

Ao Li and Yun Liu have contributed equally to the paper.

A. Li · I. Szlufarska
Materials Science Program, University of Wisconsin, Madison, WI, USA

Y. Liu
Materials Science and Engineering Department, Massachusetts Institute of Technology, Boston, MA, USA

I. Szlufarska (✉)
Department of Materials Science and Engineering, University of Wisconsin, Madison, WI, USA
e-mail: izabela@engr.wisc.edu

1 Introduction

Tribological properties (friction, adhesion, and wear) of silica are of significant importance for a number of technological applications, including wafer bonding in nanoengineering of semiconductor devices [1, 2] and wafer planarization for manufacturing of the microelectromechanical systems (MEMS) [3]. Friction and adhesion of silica are also of fundamental interest for geophysics and earthquake mechanics, since quartz is a common component of rocks and shallow tectonic earthquakes are known to result from frictional instabilities in crustal faults [4, 5]. Consequently, it is not surprising that friction of silica has been studied extensively in different contexts [6–10]. One aspect of the silica studies, which is particularly relevant to this paper, is related to the effects of surface chemistry on friction [11–13].

Silica surfaces, unlike the bulk silica, have largely lost the complete tetrahedral configuration, which gives the surface silicon atoms the tendency to bond with chemical groups [14]. Due to this tendency, hydroxyl groups (–OH) can bind to silicon atoms on silica surfaces via Si–O covalent bonds. When the concentration of the hydroxyl groups is sufficiently high, the silica surface will show a hydrophilic property and water molecules can be absorbed by forming hydrogen bonds with the surface hydroxyls [15]. When the surface chemical groups are mainly surface siloxanes (Si–O–Si), which can be achieved by dehydroxylation of the surface hydroxyls, the surface will become hydrophobic [16]. Various kinds of interactions may exist between silica surfaces, such as hydrogen bond network [11], capillary force of a condensed water meniscus [17, 18], colloidal interactions [16, 19], and covalent bonding via interfacial siloxane bridges [16], which have been reviewed in detail in Ref. [16]. These interaction

mechanisms play an important role in friction and wear of silica/silica interfaces, for example, friction increases with increasing velocity when surfaces are terminated with Si–O–Si groups and it decreases with velocity when surfaces are terminated with hydroxyl groups. The latter effect has been explained by the fact that hydroxyl groups are capable of forming H-bond networks at the interface, and a slower sliding velocity leads to formation of a stronger (more extensive) H-bond network [11]. In addition, surface damage will occur quickly during shearing of two hydrophilic silica surfaces past each other [16]. This is because silica surfaces are capable of forming strong Si–O–Si bonds across the interface through dehydroxylation reaction between two hydroxyls from each surface. These strong covalent Si–O–Si bridges can break during frictional sliding or pull atoms out of silica surfaces, which causes localized surface damage.

Atomic-level wear of silica has been previously studied in experiments that combined atomic force microscopy (AFM) and transmission electron microscopy (TEM) [20]. Specifically, the authors investigated wear between a silica surface and a silicon containing diamond like carbon (DLC) tip [20]. It was found that the classical wear law of Archard [21] fails to describe wear at the nanometer scale. The authors proposed an atom-by-atom attrition model, which was able to successfully describe the experimentally measured rate of wear of a blunted tip. The authors fitted the model to the experimental data to obtain activation energies of the elemental wear processes, but the specific atomic-level wear mechanisms were not identified. In addition, since the experiments were carried out on the interface between SiO_2 and silicon containing DLC, the wear mechanisms in these experiments may be different from those encountered at SiO_2/SiO_2 interfaces. Understanding of such mechanism is important for the development of predictive models of wear with correct activation energies. Simulations based on the molecular dynamics (MD) technique provide an excellent tool for identifying wear mechanisms directly. In the present work, we use MD to determine specific wear mechanisms that occur during shearing of two contacting silica surfaces to provide their atomic-level description.

Another interesting phenomenon related to friction and adhesion of silica reported in the last few years is that chemical reactions in silica/silica contacts can lead to contact aging [22, 23]. Aging refers to an increase in static friction as a function of time during which the surfaces are held in contact before sliding. Another manifestation of the same phenomenon is the so-called velocity weakening, which means that friction decreases with an increasing sliding velocity. Existence of velocity weakening is known to be a necessary condition for nucleation of earthquakes [4, 5]. Frictional aging has been described by a phenomenological rate and state friction laws [24, 25], which state that friction depends logarithmically on time. While this law has been validated and widely accepted, [26–29] the physical origin of frictional aging has remained a subject of debate. Two main hypotheses are plastic creep (which increases the contact area and therefore friction as a function of time) and chemical bonding (which increases adhesion as a function of time without necessarily increasing the contact area). Both of these phenomena are likely to be active in macroscopic experiments on rocks and in crustal faults, but they have been difficult to isolate from each other in laboratory experiments.

Recently, single-asperity friction experiments between amorphous silica surfaces, carried out by Li et al. [5], using AFM, demonstrated that frictional strength of nanometer-scale silica interface can increase logarithmically with the stationary holding time even in the absence of plastic deformation [5]. Specific mechanisms responsible for this chemical aging have been subsequently proposed by Liu and Szlufarska based on the results of atomistic simulations [30]. The authors excluded the hypotheses that the chemical aging observed in the AFM experiments of Li et al. [5] was due to meniscus formation or due to formation of a hydrogen bond network, as the time scales for these processes were significantly shorter than the aging time measured in experiments. It was proposed that chemical aging of silica is due to formation of strong siloxane bonds across the sliding interface. The authors of Ref. [30] employed a combination of density functional theory calculations, MD simulations based on empirical potentials, and kinetic Monte Carlo method to show that the concentration of siloxane bridges increases logarithmically with time on the time scales comparable to the aging time reported from AFM experiments. The authors also found that the energy barriers to formation of interfacial siloxane bridges on the neighboring sites are not independent of each other and that this interaction is mediated by the elastic deformation of the surrounding bulk. Friction studies were not reported in Ref. [30], and it was hypothesized that the static friction force scales linearly with the number of covalent bonds formed across the interface. This assumption has been shown to be valid before for friction between a hydrogen-passivated DLC AFM tip and hydrogen-passivated diamond sample [31, 32]. It is also expected that this assumption will be valid for the silica interfaces in the regime where the density of siloxane bridges across the interface is relatively low. For higher concentration of the siloxane bridges, it is possible that the interactions between these bridges will lead to deviations from the linear relationships between the static friction force and the number of bridges, but this dependence has not been investigated up to this point. Here, we use MD simulations to determine how static friction force at a sliding interface depends on

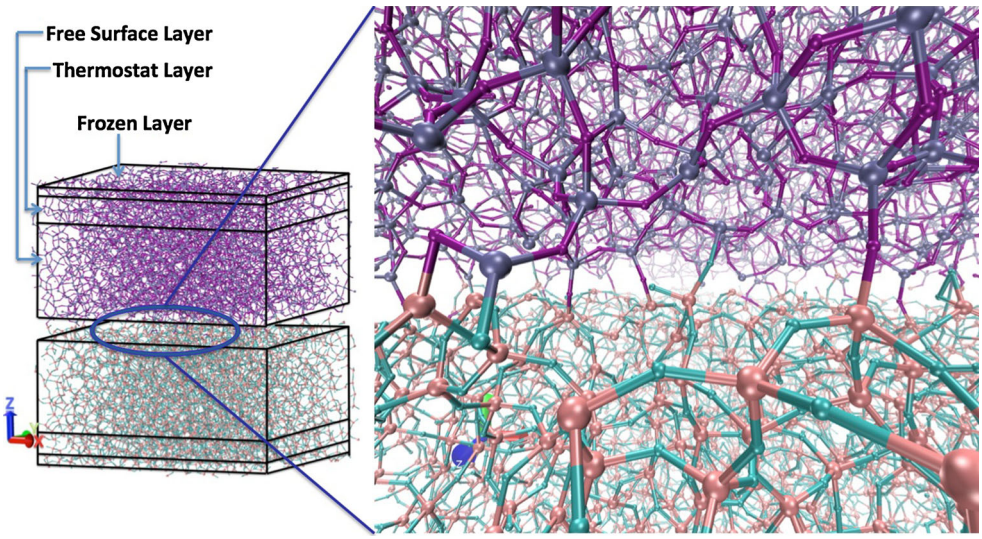

Fig. 1 Schematic picture of the simulation system with two amorphous samples (*left*) and atomistic view of the silica/silica interface between these two samples with Si–O-Si bridges (*right*). *Pink* and *cyan spheres* are silicon and oxygen atoms of the *bottom* silica sample. *Metallic blue* and *purple spheres* are Si and O atoms in the *top* silica sample

the number of siloxane bridges formed across silica/silica interface.

2 Simulation Methods

We carry out MD simulations of sliding between two silica surfaces as a function of the number of siloxane bridges formed across the sliding interface. Simulations are performed with the ReaxFF reactive force field [33], as implemented in LAMMPS [34]. We consider hydrophobic silica surfaces because hydrophobic surfaces have been shown in experiments to have a higher friction and a more apparent aging behavior than those of hydrophilic silica surfaces [16].

Figure 1 shows how one sliding interface is formed between two amorphous silica samples. Each sample (6.13 nm × 5.31 nm × 3.37 nm) consists of 2,592 silicon atoms and 5,184 oxygen atoms. It is prepared by melting the system at 5,000 K for 10 ns, quenching it down to 5 K in 20 ns, and then equilibrating for 30 ns at 5 K. Periodic boundary conditions are employed in the x and y directions (both parallel to the interface), resulting in one infinite silica/silica interface. Amorphization of the sample has been confirmed by calculating the pair distribution function. The two silica samples are referred to as the bottom and the top, respectively. All atoms in the bottom sample are divided into three groups, the bottom frozen layer, the bottom thermostat layer, and the bottom free surface layer, based on their z coordinates, where the z direction is perpendicular to the interface. Atoms in the bottom frozen layer (0 Å $< z <$ 4 Å) are not allowed to relax during the sliding simulations. Above the 4 Å-thick bottom frozen layer is an 8 Å-thick bottom thermostat layer. A velocity-rescaling algorithm is applied to atoms in this layer to explicitly rescale the temperature back to 5 K every 25 fs. Above the bottom thermostat layer is the bottom free surface layer (all atoms with z coordinates bigger than 12 Å), which is simulated with the constant energy ensemble. The top surface is modeled using a symmetric approach. An interface is formed by bringing the two surfaces together. The dimensions of the resulting silica/silica interface are 6.13 nm × 5.31 nm.

In order to prepare interfaces with different numbers of siloxane (Si–O–Si) bridges across the interface, we follow three steps. First, we performed indentation simulations continuously with the velocity of 50 m/s until the normal pressure reaches 8 GPa. The interface is then equilibrated at 5 K for 50 ps. The interface pressure is calculated by dividing the normal force acting on the interface by the nominal interfacial area. The total normal force is calculated as the sum of normal forces acting on all atoms in the top frozen layer. The reason for increasing the normal pressure is that it accelerates reactivity of the surfaces.

In the second step we facilitate chemical reactions between silica surfaces. In AFM experiments, chemical bonding of silica/silica interfaces was reported to occur on the time scale of 0.1–100 s [5, 30]. This time scale is too long for interfacial reactions to be modeled directly in MD simulations. The reason why bridge formation reaction is relatively slow is that surface silicon atoms are typically bonded to four oxygen atoms, where the oxygen atoms form a (possibly distorted) tetrahedron. Because all Si bonds are saturated in this arrangement, formation of an interfacial Si–O bridge involves first breaking of one of the surface Si–O bonds on each surface and only then formation of a Si–O–Si bridge is possible. The first step is the one that cannot be directly observed in MD simulations. Therefore, we accelerate the overall bonding process by introducing reactive sites on the surface, which means that

we remove from the surface those oxygen atoms that have dangling bonds, i.e., they are bonded only to one Si atom. As a result, the Si atom to which the O atom used to be bonded now has fewer bonds than four and therefore this Si will have a stronger tendency to from an interfacial bond. Two such under-coordinated silicon atoms from the opposite surfaces can easily form a Si–O–Si bridge, provided one oxygen atom is present in the middle between these two Si atoms and that the distances between Si and O atoms are smaller than the Si–O bond length. After removing the dangling O atoms, we search for the reactive sites on the opposite surfaces, and if the distance between two reactive Si atoms is lower than 3.6 Å (which is twice the length of the Si–O bond), we add back an oxygen atom in the middle of the distance between the two Si atoms. The interface is then relaxed one more time with ReaxFF [33], so that the actual reactions and surface relaxation are controlled by the physics of the force field. By creating different numbers of reactive sites, we can generate different number of interfacial Si–O–Si bridges after relaxations. One should note that the reactive sites are introduced to surfaces that had been first prepared and relaxed using the ReaxFF force field and therefore are expected to represent the chemistry of a realistic silica surface. In addition, although we introduce the reactive sites "by hand," these sites correspond to positions on the surface where reactions would be most likely if MD simulations were possible on longer time scales. The above scheme allows obtaining realistic silica interfaces with a controlled number of interfacial bonds. This approach is reasonable, given that our focus is not on the process of bond formation, but on the effect of the number of interfacial bonds (once they have been formed) on friction.

In the third and final step, we pull the surfaces apart continuously with a velocity of 25 m/s. During this phase, we store intermediate configurations corresponding to different normal pressures between −5.4 and −1.3 GPa. For a given interface, the number of interfacial bridges was found to be constant in this pressure range. In separate simulations, we equilibrate these intermediate configurations of silica interfaces at 5 K for 50 ps. We choose to perform simulations at the temperature of 5 K because a higher temperature would introduce unexpected fluctuations in the number of interfacial bridges, both when the interface is held still and when the surfaces are pulled apart. The above procedure results in a number of amorphous silica interfaces with different numbers of interfacial siloxane bridges and with different applied normal pressures. Figure 1 shows an example of an interface created through this scheme. An interfacial siloxane (Si–O–Si) bridge is defined using a Si–O cutoff distance of 1.8 Å, which is determined based on the position of the first minimum in the Si–O pair distribution function.

Sliding simulations are performed by moving laterally the atoms in the frozen layer of the top silica sample. Our goal was to find a sliding velocity that captures the stick–slip phenomenon, which occurs in AFM experiments on silica [5]. [16] After a series of velocity tests, we chose 75 m/s as the sliding velocity at which a clear stick–slip phenomenon can be observed. During sliding simulations, the temperature is kept at 5 K because we want to isolate the effect of the chemistry of the interface (concentration of the interfacial bridges) on friction from the effects of temperature. At higher temperatures, bond breaking could take place due to thermal activations. Friction force is calculated by summing lateral forces on all atoms in each frozen layer and then by averaging it over the two frozen layers. We average the friction forces over multiple sliding directions and over different equilibration times of prepared interfaces. The numbers over which the results are averaged are provided in the results section.

3 Results

3.1 Dependence of Static Friction F_s on the Number of Interfacial Bridges

The static friction force F_s can be determined by plotting the lateral friction force F_L as a function of the sliding distance. An example of such a plot is shown in Fig. 2. Sliding distance is defined as the lateral displacement of the center of mass of the top frozen layer, which is displaced laterally at a constant velocity. Initially, the silica surfaces stick to each other and the friction force increases. The maximum force corresponds to the static friction force F_s.

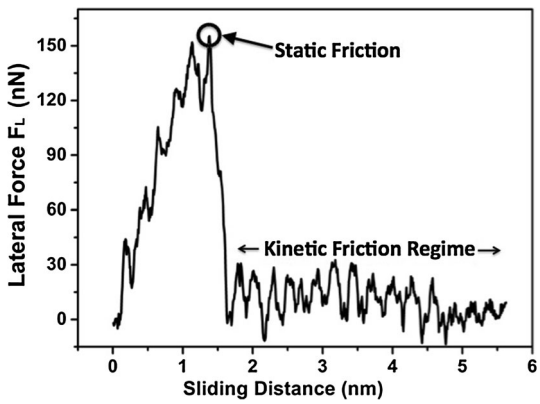

Fig. 2 Typical lateral relationship between the friction force F_L and the sliding distance measured in MD simulations. Here, the initial number of siloxane bridges across the interface before sliding is 19, which corresponds to a concentration of 0.58 nm^{-2}. The initial normal pressure before sliding is −4.76 GPa (adhesive). The maximum of F_L, marked with an *open circle* corresponds to the static friction force F_s

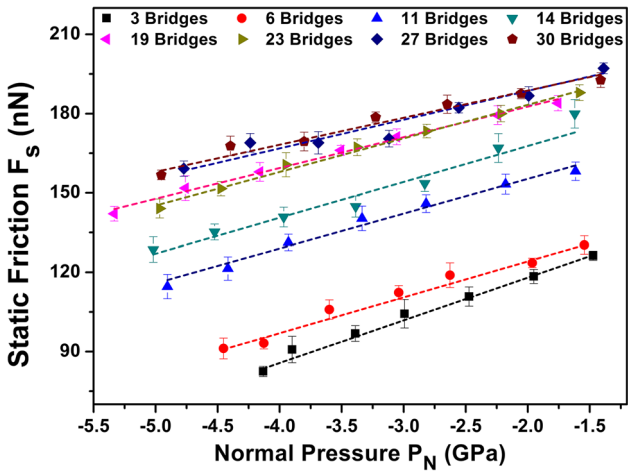

Fig. 3 (Color online) Dependence of the static friction F_s on the applied normal pressure P_N. The interfacial area is equal to 32.55 nm^2. *Symbols* correspond to interfaces with different number of interfacial siloxane bridges. *Dashed lines* represent linear fits

Our simulations reveal that at this point all the interfacial bridges break almost simultaneously and then the interface slips. Correspondingly, the resistance to sliding F_L decreases (see Fig. 2).

In order to understand the effects of the concentration of siloxane bridges on static friction of amorphous silica, we prepare amorphous silica interface with 3, 6, 11, 14, 19, 23, 27, and 30 siloxane bridges, which corresponds to bridge concentrations of 0.092, 0.184, 0.338, 0.43, 0.58, 0.71, 0.83, and 0.92 bridges per nm^2, respectively. Normal pressure P_N is controlled by changing the distance between frozen layers of the top and the bottom silica samples, as described in Section II. By plotting F_L versus sliding distance for each bridge concentration and for each value of normal pressure, we determine the static friction F_s as a function of P_N. The results are shown in Fig. 3. The major feature of Fig. 3 is that for each interface with a given number of siloxane bridges, F_s increases linearly with P_N. The reported values of F_s for interfaces with 3, 6, 11, and 14 bridges are averaged over six sliding simulations where we vary the sliding direction and the interface equilibration time. The values of F_s for interfaces with 19, 23, 27, and 30 bridges are averaged over eight independent sliding simulations. The error bar corresponds to the 70 % confidence interval of the fitted values using Student's t distribution. The dashed lines represent fits of F_s versus P_N for each interface. The parameters of the linear fit for F_s versus P_N relationship are given in Table 1. The negative values of P_N in Fig. 3 mean that the adhesive forces dominate the interaction due to stretching of interfacial bridges. We choose the negative P_N regime because higher values of P_N can lead to a gradual disappearance of a distinct static friction regime in our simulations.

Table 1 Parameters of a linear fit $y = a + bx$ to the relationship between the static friction force F_s and the normal pressure P_N

Number of bridges	a	σ_a	b	σ_b	R^2
3	150.309	1.318	16.160	0.453	0.995
6	151.271	1.608	13.578	0.521	0.976
11	181.608	2.275	13.154	0.678	0.980
14	194.799	2.784	13.553	0.755	0.939
19	205.965	1.810	11.644	0.494	0.990
23	208.769	1.825	12.716	0.534	0.994
27	210.381	1.372	10.893	0.458	0.947
30	209.239	1.312	10.261	0.372	0.975

σ_a, and σ_b are the standard deviations of a, and b, respectively. R^2 represents the goodness of the fit

The linear relationship between F_s and P_N can be understood in light of a one-dimensional the Prandlt–Tomlinson model [35]. We define $V(x)$ as the interaction energy between the top and the bottom silica samples, where x is the displacement of the lower surface of the top silica sample along the direction of sliding. The elastic energy stored in the top silica sample can be written as $E_{el}(x) = \frac{1}{2}k(X - x)^2$, where k is the effective spring constant and X is the lateral displacement of the frozen layer of the top silica sample along the direction of sliding (see Sect. 2). If we neglect inertia, the total energy of the top silica sample $E_{tot}(x)$ is equal to the sum of the energy due to interactions with the bottom silica sample $V(x)$ and the elastic energy E_{el} stored in the top silica sample, as shown in the following equation

$$E_{tot}(x) = V(x) + \frac{1}{2}k(X - x)^2 \quad (1)$$

Figure 4 is a schematic representation of the energy landscape $V(x)$ of the top silica sample. The $V(x)$

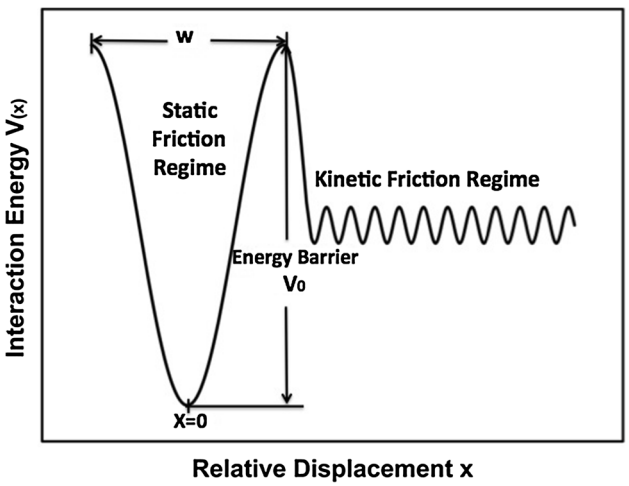

Fig. 4 Schematic energy landscape $V(x)$ representing the interaction energy between the *top* and the *bottom* silica sample. x is the lateral displacement of the lower surface of the *top* silica sample

landscape corresponds to the data shown in Fig. 2, where there is a clear transition from static to kinetic friction. $V(x)$ reaches a minimum value when $x \approx 0$, which corresponds to the initial state of the interface before frictional sliding. In this state, the interface is stable and the interfacial bridges are not strained or broken due to frictional sliding. When x increases, the interfacial bridges that connect the surfaces of the top and the bottom silica samples are increasingly strained, which in turn leads to an increase in $V(x)$. Eventually, the interfacial bonds break, which corresponds to the maximum energy barrier V_0. In our simulations, we observe all bonds breaking during the stick–slip transition. After the stick–slip transition, the system enters the regime of kinetic friction. In the kinetic friction regime, bond-forming and bond-breaking reactions also happen during frictional sliding, which leads to the corrugated $V(x)$ in this regime. As a result, the $V(x)$ minima in the kinetic regime are not as low as the energy of the initial state $V(0)$, and the maxima of $V(x)$ in the kinetic regime are not as high as the energy V_0 corresponding to the initial breaking of bonds.

In this paper, we are primarily interested in the static regime of friction. We define w as the peak-to-peak width of the potential energy well in the static friction regime (see Fig. 4). We approximate $V(x)$ in the interval $-\frac{w}{2} < x < \frac{w}{2}$ using the following relation [36]

$$V(x) = -\frac{V_0}{2}\cos\left(\frac{2\pi}{w}x\right). \tag{2}$$

In this static friction regime, we can assume the lateral force F_L to be linear with $(X - x)$, which represents the lateral deformation of the top silica sample due to shearing. F_L can therefore be written as

$$F_L = k(X - x). \tag{3}$$

In a quasi-static motion, $E_{tot}(x)$ of the top silica sample remains in a local minimum. The two conditions for determining a local minimum are as follows:

$$E'_{tot}(x) = V'(x) - k(X - x) = 0 \tag{4}$$

$$E''_{tot}(x) > 0. \tag{5}$$

$E'_{tot}(x)$ and $E''_{tot}(x)$ are the first and the second derivatives of $E_{tot}(x)$ with respect to x, respectively. [35] Combing Eqs. (2), (3), and (4), we obtain

$$F_L = \frac{\pi V_0}{w}\sin\left(\frac{2\pi x}{w}\right) \tag{6}$$

in the interval $-\frac{w}{2} < x < \frac{w}{2}$. The static friction F_s can be measured by determining the maximum absolute value of the lateral force $|F_L|_{max}$ in the entire sliding process [36]. Based on Eq. (6), the static friction force is equal to $|F_L|_{max}$ when $x = w/4$, that is,

$$F_s = |F_L|_{max} = \frac{\pi V_0}{w}. \tag{7}$$

Equation (7) satisfies both conditions given by Eqs. (4) and (5). Now, according to the Eyring model [37], the energy barrier V_0 for breaking of interfacial siloxane bridges can be modified by the mechanical work done on the system

$$V_0 = \Delta U_{act} + \sigma_n \Delta V_{act} \tag{8}$$

where ΔU_{act} is the stress-free energy barrier for breaking of all existing interfacial bonds, σ_n is the applied normal stress, and ΔV_{act} is the activation volume. ΔV_{act} is assumed to be constant in our system, which is justified based on published density functional theory calculations for siloxane bridge formation at silica/silica interface (see Supplemental Information in Ref [30]) and by experimental measurements of sliding friction at other interfaces [38] [39]. As shown by Eq. (8), σ_n increases the energy barrier. One should keep in mind that our simulations are carried out in the adhesive regime, which means that σ_n is negative. By plugging in Eq. (8) into Eq. (7), we obtain

$$F_s = \frac{\pi \Delta U_{act}}{w} + \frac{\pi \sigma_n \Delta V_{act}}{w} = \frac{\pi \Delta U_{act}}{w} + \frac{\pi \Delta V_{act}}{w} P_N \tag{9}$$

P_N is the applied normal pressure, which equals to the normal stress σ_n. As shown by Eq. (9), the static friction F_s depends linearly on the applied normal pressure P_N, which is consistent with the linear relationship observed in our simulations and is shown in Fig. 3.

An important question that remains to be answered is the dependence of the static friction force on bridges concentration at silica interfaces. As shown in Fig. 3, the increase in both, the applied normal pressure and the number of interfacial bridges, leads to an increase in the static friction force. In order to isolate the effects of the number of siloxane bridges from the effects of the applied normal pressure, in Fig. 5, we plot the static friction force F_s as a function of the number of bridges n at a constant normal pressure. Each data point corresponds to the static friction force predicted by the linear fits in Fig. 3 for a given value of the normal pressure. Figure 5 shows that F_s increases with n with a decreasing slope. Although for low values of n this relationship can be approximated as a linear function, significant deviations from the linear behavior are observed for intermediate and large values of n. The error bar in Fig. 5 corresponds to the 70 % confidence interval of each data point using error propagation.

To understand why the derivative of F_s with respect to n decreases in the regime of large bridge concentration, it is useful to consider how the value of n affects the energy barrier V_0 for breaking interfacial bridges during sliding. As reported in Ref. [30], increasing n leads to an increase

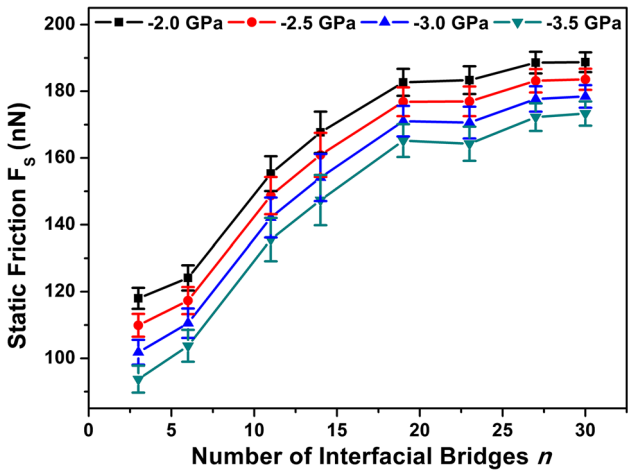

Fig. 5 (Color online) Dependence of the static friction F_s on the number of interfacial bridges n. The interfacial area is equal to 32.55 nm^2. *Symbols* (and *colors* online) correspond to different applied normal pressures. The *lines* connecting data points are added to guide the eye

in the reaction energy for formation of a new siloxane bridge across the interface. We define $\Delta\text{Eform}, i$ to be the energy to form a siloxane bridge i across the interface. If we assume that the bridge breaking process is the opposite process to bridge formation, then the reaction energy of breaking a bridge i is $\Delta\text{Ebreak}, i = -\Delta\text{Eform}, i$. Based on the Bronsted–Evans–Polanyi (BEP) relation [37], we assume a linear relationship between reaction energy and reaction energy barriers.

$$V_{0,\text{break},i} = \alpha \cdot \Delta\text{Ebreak}, i + g = -\alpha \cdot \Delta\text{Eform}, i + g \qquad (10)$$

In the above expression, $V_{0,\text{break},i}$ is the energy barrier for breaking the bridge i, and α and g are constant parameters in the BEP relation. The factor α is between 0 and 1, and it characterizes the position of the transition state along the reaction coordinate. We also assume that all n interfacial bridges break simultaneously (which is justified by observations from our MD simulations) and that all bridges have the same energy barrier for bond breaking. The latter supposition simplifies the mathematical derivation without changing the resulting qualitative trends. We then obtain

$$V_0 = \sum_{i=1}^{n} V_{0,\text{break},i} = n \cdot V_{0,\text{break},i} \qquad (11)$$

Plugging in Eqs. (10) and (11) into Eq. (7), we get

$$F_s = \frac{\pi V_0}{w} = \frac{\pi \cdot n \cdot V_{0,\text{break},i}}{w} = \frac{-\alpha\pi \cdot \Delta\text{Eform}, i + g\pi}{w} \cdot n \qquad (12)$$

From both, Eq. (12) and from Ref. [31], $\Delta\text{Eform}, i$ increases with n and therefore $\frac{-\alpha\pi \cdot \Delta\text{Eform},i+g\pi}{w}$ decreases with n. This is consistent with the trend observed in Fig. 5 and shows that the force needed to break a siloxane bridge becomes smaller when the bridge concentration is larger.

3.2 Atomic-Level Wear Mechanisms

We investigate the atomic-level mechanisms of wear that took place in our MD simulations. Two most common mechanisms are shown in Fig. 6a1–a3, b1–b6). Figure 6a1–a3 shows wear by transfer of an individual atom. By shearing the silica/silica interface, the preexisting interfacial Si–O–Si bridge (Fig. 6a1) becomes stretched and broken through the rupture of one of the Si–O bonds of the siloxane bridge (Fig. 6a2). As a result, the oxygen atom that used to be bonded to the top silica surface is pulled to the bottom silica surface by the remaining Si–O bond of the siloxane. Subsequently, the transferred oxygen atom forms a surface siloxane bridge on the bottom silica surface and becomes chemically non-reactive (Fig. 6a3). This wear mechanism by individual oxygen atom transfer is most common because it involves breaking of only one Si–O bond, as opposed to mechanisms that involve breaking of multiple bonds, such as pulling out a Si atom or the entire cluster of atoms from the silica surface.

However, when shearing two surfaces past each other, not all bond breakings occur in the interfacial siloxanes and some surface Si–O bonds will also be broken, which eventually will build up damage and lead to a transfer of the entire atomic cluster. Figure 6b1–b6 illustrates how an atomic cluster is nucleated, how it grows, and finally how it is transferred to the counter surface. The Si atom marked by the red arrow is initially bonded to three O atoms in the bottom surface (Fig. 6b1). Due to shearing of the surfaces, local stress near the silicon atom accumulates and leads to breaking of two of the three Si–O bonds that hold the Si atom to the bottom silica surface (see Fig. 6b2). The silicon atom becomes highly reactive as it now participates in only one covalent bond. Moreover, without the geometric constraint of the tetrahedron that is typical of silica structure, the Si atom in question can move closer to the top silica surface than before, which makes it easier for this atom to react with oxygen atoms from the top silica surface. In Fig. 6b3, the Si atom has attracted an O atom (marked by blue arrow in Fig. 6b2, b3) and is pulling it out from the top silica surface. This protruding cluster (marked by a black circle) consists of a linear chain of three Si–O bonds and therefore is chemically highly reactive. The group of atoms circled in green in Fig. 6b3 is another interfacial SiO_3 cluster with part of tetrahedron structure, formed through bonding reactions from two single oxygen atoms (marked by black arrows in Fig. 6b2) and a Si–O cluster (marked by green circle in Fig. 6b2) during the sliding process. When these two clusters get close enough, they

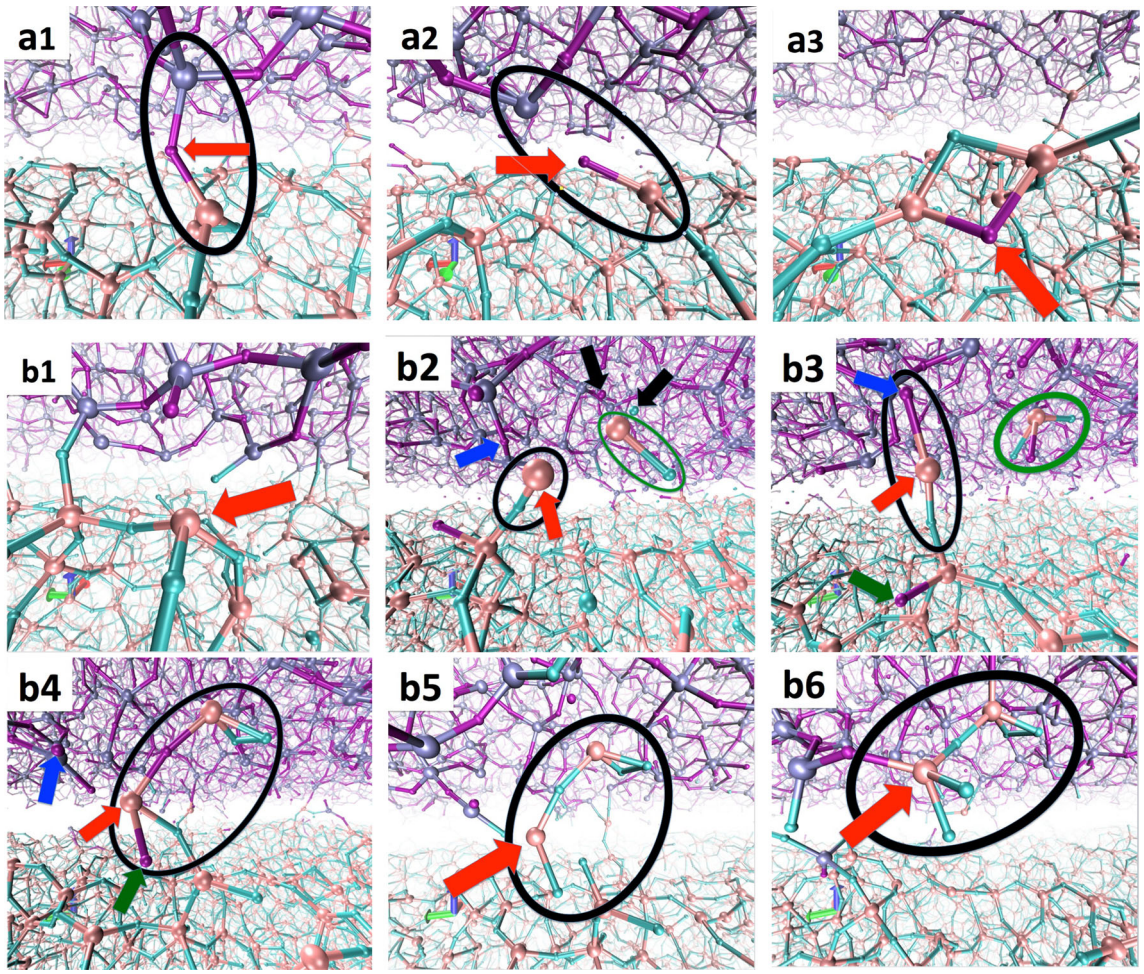

Fig. 6 Atomic scale wear mechanisms of silica/silica interface. **a1–a3** show a wear mechanism by transfer of an individual oxygen atom accompanied by breaking of one Si–O bond in the interfacial siloxane bridge. **b1–b6** show a wear mechanism by transfer of an atomic cluster. In all *panels*, *pink* and *cyan spheres*, respectively, are Si and O atoms of the *bottom* silica sample. *Metallic blue* and *purple spheres*, respectively, are Si and O atoms of the *top* silica sample. *Red arrow* in **a1–a3** marks O atom that is at the center of an interfacial siloxane bridge. *Red arrow* in **b1–b6** *marks* Si atom that is being transferred from the *bottom* to the *top* silica samples. *Blue*, *black*, and *green arrows* in **b2–b4** each marks a specified oxygen atom involved in cluster formation and transfer. *Black* and *green circles* show clusters participating in the material transfer during wear, as explained in detail in the main text

react and bond, forming one bigger cluster that consists of two Si and four O atoms (Fig. 6b4). This Si_2O_4 cluster also shows imperfect tetrahedron structure (i.e., one atom is missing from the tetrahedron) and is connected with the bottom silica sample with only one Si–O bond. In Fig. 6b5, the newly formed bigger cluster leaves the bottom silica surface by breaking the remaining Si–O bond that holds it to the bottom silica surface and there are no covalent bonds between this cluster and the two silica surfaces. Finally, the cluster is incorporated into the top silica surface by forming new Si–O bonds (see Fig. 6b6).

Although the details of the transfer vary between different wear events, there are some general features that are characteristic of such transfers, as observed in our simulations. We find that Si atoms become reactive due to breaking of surface Si–O bonds. These reactive silicon atoms have a strong tendency either to bond to oxygen atoms from the opposite surface or to attract and bond interfacial atomic clusters. If an atomic cluster breaks off from a surface, it becomes an interfacial debris particle, which can slide or roll in the interfacial space. Interfacial clusters are highly reactive, and they can be reabsorbed by one of the surfaces. In the case where the cluster is absorbed by the counter surface (instead of the original surface from which it was removed), it becomes a transferred cluster. The clusters are nucleated and dissolved continually during the sliding process. They play an important role in the friction and wear of silica/silica interface because they can form more Si–O bonds across the interface than a single siloxane bridge. These

Table 2 Percentage of transfer events underlying wear that involve a cluster of size S

Number of interfacial bridges	$S = 1$	$S = 2$	$S = 3$	$S = 4$	$S = 5$	$S = 6$	$S \geq 7$	$N_{transfer}$
3	83.8 ± 6.0	8.6 ± 0.8	2.9 ± 0.4	1.9 ± 0.4	2.9 ± 0.8	0.0 ± 0.0	0.0 ± 0.0	17.5 ± 0.25
6	82.1 ± 5.2	10.3 ± 1.8	4.3 ± 0.7	0.9 ± 0.3	0.9 ± 0.3	0.9 ± 0.3	0.9 ± 0.3	19.5 ± 0.21
11	73.1 ± 5.7	10.3 ± 1.4	9.5 ± 0.9	4.3 ± 0.5	0.9 ± 0.2	0.9 ± 0.4	0.9 ± 0.4	19.4 ± 0.49
14	75.5 ± 5.5	12.2 ± 1.1	10.7 ± 0.9	1.5 ± 0.4	0.0 ± 0.0	0.0 ± 0.0	0.0 ± 0.0	21.8 ± 0.42
19	69.6 ± 2.4	12.1 ± 1.4	8.2 ± 1.7	6.3 ± 1.1	1.5 ± 0.6	1.5 ± 0.7	1.0 ± 0.5	25.9 ± 1.20
23	68.2 ± 3.1	13.6 ± 1.5	8.0 ± 1.2	5.3 ± 0.9	3.4 ± 1.6	1.1 ± 0.5	0.4 ± 0.4	33.0 ± 0.63
27	73.6 ± 1.6	10.0 ± 0.7	7.8 ± 0.8	5.0 ± 1.2	1.2 ± 0.8	0.0 ± 0.0	2.4 ± 0.8	40.1 ± 1.76
30	73.2 ± 0.9	11.3 ± 1.2	7.9 ± 1.2	4.5 ± 1.2	1.4 ± 0.4	0.6 ± 0.3	1.1 ± 0.8	44.4 ± 2.42

The reported values correspond to averages over 56 simulations, and the uncertainty corresponds to a standard deviation from this average. $N_{transfer}$ represents the total number of transfer events for the interface size of 32.55 nm^2

conclusions are based on the analysis of images from approximately 100 sliding simulations.

We can quantify contributions of the above mechanisms to wear by comparing the atomic structure of the interface before sliding with the structure after 50 ps of sliding. Specifically, we identify atoms that used to belong to one of the surfaces before sliding and are transferred during sliding to the opposite surface. This analysis is performed for 56 sliding simulations and below we report the average values. Not surprisingly, we found that the total number of transferred atoms (individually or as part of a cluster) increases significantly with the number of interfacial bridges formed before sliding. This number changes from $(46 \pm 2) \times 10^{-2}$ atoms per nm^2 for the case $n = 3$ interfacial bridges to $(138 \pm 4) \times 10^{-2}$ atoms per nm^2 for the case of $n = 30$, where the uncertainty corresponds to a standard deviation from this average. In Table 2, we also provide information about the percentage of events in which atoms have been transferred individually or in a cluster of size S. Although many more simulations would be needed to obtain more quantitative trends (which is beyond the scope of this paper), data in Table 2 has a number of qualitative trends. These trends are also shown in Fig. 7. Specifically, the majority of wear transfer events involve individual atoms ($S = 1$). In addition, there are non-negligible contributions to wear transfer from clusters of up to size four. For these clusters, the percentage of events generally decreases with an increasing size of the cluster. Although we do observe events involving cluster of size $S > 4$, the number of these events is quite small with no clear trend with the cluster size. We also find that when the number of initial interfacial bridges increases, the percentage of transfers involving a single atom generally decreases and the total contributions to wear from clusters ($S > 1$) increases. The total number of transfer events $N_{transfer}$ is also found to increase with the initial number of interfacial bridges, as is shown in Table 2.

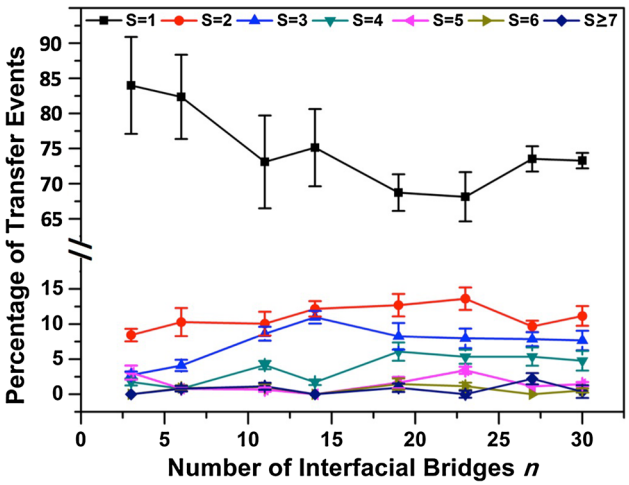

Fig. 7 Percentage of wear events in which atoms were transferred individually ($S = 1$) or in a cluster of size S ($S \geq 2$). *Error bars* correspond to 70 % confidence interval

4 Conclusion

We find that for two flat silica surfaces with the same siloxane bridge concentration, the static friction between them increases linearly with the normal pressure (and therefore also with load). We also find that the static friction force increases nonlinearly with the concentration of interfacial siloxane bridges, which can be explained by interactions among neighboring bridges. By analyzing atomic scale wear mechanisms of silica/silica interface, we demonstrated two dominant wear mechanisms which are individual oxygen atom transfer accompanied by breaking one of Si–O bonds in the interfacial siloxane bridges, and by atomic-cluster transfers initialized by ruptures of surface siloxane bridges. Small clusters are continually formed and dissolved at the sliding interface, which play an important role in wear of silica/silica interface.

Acknowledgment The authors acknowledge helpful discussions with Professor Robert Carpick, Professor Terry Tullis, Dr. David Goldsby, and Professor Qunyang Li. This work is supported by NSF Grant No. EAR-0910779 and the Army Research Office Grant No. W911NF-12-1-0548.

References

1. Lasky, J.B.: Wafer bonding for silicon-on-insulator technologies. Appl. Phys. Lett. **48**, 78–80 (1985)
2. Ventosa, C., Rieutord, F., Libralesso, L., Morales, C., Fournel, F., Moriceau, H.: Hydrophilic low-temperature direct wafer bonding. J. Appl. Phys. (2008). doi:10.1063/1.3040701
3. Taran, E., Donose, E., Vakarelski, I.U., Higashitani, K.: pH dependence of friction forces between silica surfaces in solutions. J. Colloid Interface Sci. **297**, 199–203 (2006)
4. Scholz, C.: Earthquakes and friction laws. Nature **391**, 37–42 (1998)
5. Li, Q., Tullis, T.E., Goldsby, D., Carpick, R.W.: Frictional ageing from interfacial bonding and the origins of rate and state friction. Nature **480**, 233–236 (2011)
6. Chandross, M., Webb III, E.B., Stevens, M.J., Grest, G.S.: Systematic study of the effect of disorder on nanotribology of self-assembled monolayers. Phys. Rev. Lett. (2004). doi:10.1103/PhysRevLett.93.166103
7. Chandross, M., Lorenz, C.D., Stevens, M.J., Grest, G.S.: Simulations of nanotribology with realistic probe tip models. Langmuir **24**, 1240–1246 (2008)
8. Toro, G.D., Goldsby, D.L., Tullis, T.E.: Friction falls towards zero in quartz rock as slip velocity approaches seismic rates. Nature **427**, 436–439 (2004)
9. Xu, J., Kato, K.: Formation of tribochemical layer of ceramics sliding in water and its role for low friction. Wear **245**, 61–75 (2000)
10. Heim, L., Blum, J., Preuss, M., Butt, H.: Adhesion and friction forces between spherical micrometer-sized particles. Phys. Rev. Lett. **16**, 3328–3331 (1999)
11. Chen, J., Ratera, I., Park, J., Salmeron, M.: Velocity dependence of friction and hydrogen bonding effects (2006). doi:10.1103/PhysRevLett.96.236102
12. Subhalakshmi, K., Devaprakasam, D., Math, S., Biswas, S.K.: Use of Eyring equation to explore the frictional responses of a –CF3 and a –CH3 terminated monolayers self-assembled on silicon substrate. Tribol. Lett. **32**, 1–11 (2008)
13. Taran, E., Kanda, Y., Vakarelski, I.U., Higashitani, K.: Nonlinear friction characteristics between silica surfaces in high pH solution. J. Colloid Interface Sci. **307**, 425–432 (2007)
14. Zhuravlev, L.T.: The surface chemistry of amorphous silica. Zhuravlev model. Colloids Surf. Physicochem. Eng. Asp. **173**, 1–38 (2000)
15. Plößl, A., Kräuter, G.: Wafer direct bonding: tailoring adhesion between brittle materials. Mater. Sci. Eng. R **25**, 1–88 (1999)
16. Vigil, G., Xu, Z., Steinberg, S., Israelachvili, J.: Interactions of silica surfaces. J. Colloid Interface Sci. (1994). doi:10.1006/jcis.1994.1242
17. Riedo, E., Lévy, F., Brune, H.: Kinetics of capillary condensation in nanoscopic sliding friction. Phys. Rev. Lett. (2002). doi:10.1103/PhysRevLett.88.185505
18. Szoszkiewicz, R. Riedo, E.: Nucleation time of nanoscale water bridges. Phys. Rev. Lett. (2005). doi:10.1103/PhysRevLett.95.135502
19. Adler, J.J., Rabinovich, Y.I., Moudgil, B.M.: Origins of the non-DLVO force between glass surfaces in aqueous solution. J. Colloid Interface Sci. **237**, 249–258 (2001)
20. Bhaskaran, H., Gotsmann, B., Sebastian, A., Drechsler, U., Lantz, M.A., Despont, M., Jaroenapibal, P., Carpick, R.W., Chen, Y., Sridharan, K.: Ultralow nanoscale wear through atom-by-atom attrition in silicon-containing diamond-like carbon. Nat. Nanotechnol. **5**, 181–185 (2010)
21. Archard, J.F.: Contact and rubbing of flat surfaces. J. Appl. Phys. **24**, 981–988 (1953)
22. Bocquet, L., Charlaix, E., Ciliberto, S., Crassous, J.: Moisture-induced ageing in granular media and the kinetics of capillary condensation. Nature **396**, 735–737 (1998)
23. Dieterich, J.H.: Time-dependent friction in rocks. J. Geophys. Res. **77**, 3690–3697 (1972)
24. Ruina, A.: Slip instability and state variable friction laws. J. Geophys. Res. **88**, 10359–10370 (1983)
25. Dieterich, J.: Modeling of rock friction: 1. Experimental results and constitutive equations. J. Geophys. Res. **84**, 2161–2168 (1979)
26. Capozza, R., Barel, I., Urbakh, M.: Probing and tuning frictional aging at the nanoscale. Sci. Rep. (2013). doi:10.1038/srep01896
27. Beeler, N.M.: Review of the physical basis of laboratory-derived relations for brittle failure and their implications for earthquake occurrence and earthquake nucleation. Pure Appl. Geophys. **161**, 1853–1876 (2004)
28. Nakatani, M., Scholz, C.: Frictional healing of quartz gouge under hydrothermal conditions: 2. Quantitative interpretation with a physical model. J. Geophys. Res. (2004). doi:10.1029/2003JB002938
29. Rice, J.R., Lapusta, N., Ranjith, K.: Rate and state dependent friction and the stability of sliding between elastically deformable solids. J. Mech. Phys. Solids **49**, 1865–1898 (2001)
30. Liu, Y., Szlufarska, I.: Chemical origins of frictional aging. Phys. Rev. Lett. (2012). doi:10.1103/PhysRevLett.109.186102
31. Mo, Y., Turner, K.T., Szlufarska, I.: Friction laws at the nanoscale. Nature **457**, 1116–1119 (2009)
32. Mo, Y., Turner, K.T., Szlufarska, I.: Origin of the isotope effect on solid friction. Phys. Rev. B (2009). doi:10.1103/PhysRevB.80.155438
33. Fogarty, J.C., Aktulga, H.M., Grama, A.Y., van Duin, A.C.T., Pandit, S.A.: A reactive molecular dynamics simulation of the silica-water interface. J. Chem. Phys. (2010). doi:10.1063/1.3407433
34. Plimpton, S.: Fast parallel algorithms for short-range molecular dynamics. J. Comput. Phys. (1995). doi:10.1006/jcph.1995.1039
35. Hölscher, H., Schirmeisen, A., Schwarz, U.D.: Principles of atomic friction: from sticking atoms to superlubric sliding. Philos. Trans. A Math. Phys. Eng. Sci. **366**, 1383–1404 (2008)
36. Socoliuc, A., Bennewitz, R., Gnecco, E., Meyer, E.: Transition from stick-slip to continuous sliding in atomic friction: entering a new regime of ultralow friction. Phys. Rev. Lett. (2004). doi:10.1103/PhysRevLett.92.134301
37. Evans, M., Polanyi, M.: Some applications of the transition state method to the calculation of reaction velocities, especially in solution. Trans. Faraday Soc. **31**, 875–894 (1935)
38. Riedo, E., Gnecco, E., Bennewitz, R., Meyer, E., Brune, H.: Interaction potential and hopping dynamics governing sliding friction. Phys. Rev. Lett. (2003). doi:10.1103/PhysRevLett.91.084502
39. Furlong, O.J., Manzi, S.J., Pereyra, V.D., Bustos, V., Tysoe, T.: Monte Carlo simulations for Tomlinson sliding models for non-sinusoidal periodic potentials. Tribol. Lett. **39**, 177–180 (2010)